Dalton Transactions

PAPER

View Article Online
View Journal

Cite this: DOI: 10.1039/c4dt02954b

Argentivorous molecules bearing three aromatic side arms: synthesis of triple-armed cyclens and their complexing property towards Ag^+†

Yoichi Habata,*[a,b] Juli Kizaki,[a] Yasuhiro Hosoi,[a] Mari Ikeda[b,c] and Shunsuke Kuwahara[a,b]

Received 25th September 2014,
Accepted 7th November 2014

DOI: 10.1039/c4dt02954b

www.rsc.org/dalton

Triple-armed cyclens bearing three aromatic side-arms were prepared in three steps from (3*R*,5*S*)-3,5-dimethyl-1,4,7,10-tetraazacyclododecane-2,6-dione, and the Ag^+-ion-induced ^1H NMR and UV-vis spectral changes and X-ray structures suggested that the aromatic side-arms cover the Ag^+ incorporated into the ligand cavities like an insectivorous plant (Venus flytrap).

Introduction

In the last decade, cyclen has been widely used as an ion recognition site in metal ion sensors, as a building block for supramolecular structures, in catalytic drugs, chirality signaling, MRI and fluorescent probes for imaging and so on.[1] Recently, we have reported[2] that tetra-armed and double-armed cyclens with aromatic side-arms behave like an insectivorous plant (Venus flytrap) when they form complexes with Ag^+. The aromatic side-arms in the armed-cyclens cover the Ag^+ incorporated into the cyclen cavities by Ag^+–π and CH–π interactions in an organic solvent as well as in water. The diameter of the cavity of cyclen, which is a 12-membered ring, is small for Ag^+, and an Ag^+ ion incorporated into the cyclen unit is exposed on the surface of the cyclen ring to allow Ag^+–π interactions between the Ag^+ and the aromatic side-arms. This behavior is not observed in Ag^+ complexes with benzyl-armed diaza-18-crown-6 ethers[3] because CH–π interactions between aromatic rings are not possible in the diaza-18-crown-6 ether derivatives. We named the armed cyclens "argentivorous molecules".[4] The aromatic side-arms in tetra-armed cyclens cover the Ag^+ incorporated into the cyclen cavity, even though electron withdrawing groups such as F, NO_2, and COO^- groups are introduced onto the phenyl rings, all four aromatic side-arms cover the Ag^+ in the tetra-armed cyclens. On the other hand, the double-armed cyclens bearing naphthalene, anthracene, and pyrene which have higher electron density than substituted benzenes cover the Ag^+, however the double-armed cyclens bearing phenyl rings as side-arms do not cover the Ag^+.[2d] These results indicate that Ag^+–π interactions between the Ag^+ and aromatic side-arms as well as CH–π interactions between neighboring aromatic rings are important for the dynamic conformational changes in the armed-cyclens. In continuation of our previous work, we prepared triple-armed cyclens in order to answer the following questions: (i) in triple-armed cyclens bearing three phenyl rings, whether the aromatic side-arms cover the Ag^+ or not. (ii) If the aromatic side-arms cover the Ag^+ in the triple-armed cyclens, when a combination of two kinds of aromatic rings is introduced into a cyclen as a side-arm, whether the substituent effects on the phenyl groups can be observed or not. (iii) In the tetra-armed cyclens, some Ag^+ complexes were a mixture of Δ and Λ forms in the solid state as shown in Fig. 1. The CH–π interactions in triple-armed cyclen/Ag^+ complexes may be weaker than those in tetra-armed cyclen/Ag^+ complexes because triple-armed cyclens lack one aromatic ring. Therefore, we expected that inversion of the side-arms (Δ and Λ forms) would be observed. During research efforts on the study of tetra-armed cyclens with two chiral centers on the cyclen ring, we found that (3*R*,5*S*)-3,5-dimethyl-1,4,7,10-tetraazacyclododecane-2,6-dione (*meso*-**6**) affords triple-armed cyclens selectively. Here, we report the synthesis of triple-armed cyclens with two methyl groups, the structures of Ag^+ complexes in solution and in the solid state, and the inversion barrier of the Δ and Λ forms.

[a]*Department of Chemistry, Faculty of Science, Toho University, 2-2-1 Miyama, Funabashi, Chiba 274-8510, Japan. E-mail: habata@chem.sci.toho-u.ac.jp*
[b]*Research Center for Materials with Integrated Properties, Toho University, 2-2-1 Miyama, Funabashi, Chiba 274-8510, Japan*
[c]*Education Center, Faculty of Engineering, Chiba Institute of Technology, 2-1-1 Shibazono, Narashino, Chiba 275-0023, Japan*

† Electronic supplementary information (ESI) available: Spectral data for the synthesized compounds and (PDF); crystallographic data for *meso*-**6**, *meso*-**9a**/$AgClO_4$, *meso*-**9c**/$AgPF_6$, and *meso*-**9d**/$AgClO_4$ (CIF). CCDC 1025463–1025466. For ESI and crystallographic data in CIF or other electronic format see DOI: 10.1039/c4dt02954b

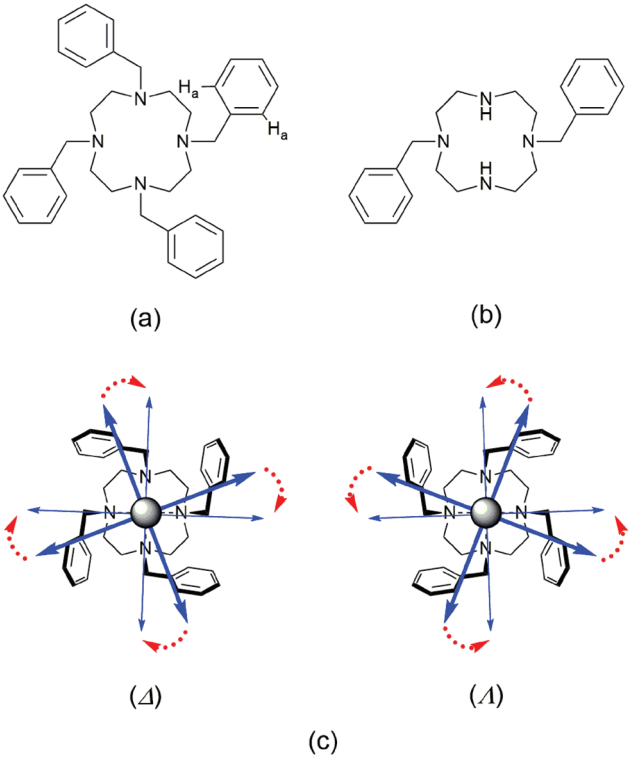

Fig. 1 Tetra-armed (a) and double-armed (b) cyclens bearing benzenes as side-arms. Definition of the Δ and Λ forms in tetra-armed cyclens (c).

Results and discussion

Triple-armed cyclens were prepared as follows: (*S*)-(−)-lactic acid tosylate ((*S*)-**2**)[5] and ethyl L-alaninate ((*S*)-**4**)[6] were prepared from (*S*)-(−)-lactic acid and L-alanine, respectively.

(2*S*,2′*R*)-Diethyl 2,2′-iminodipropionate (*meso*-**5**)[7] was prepared by the reaction of (*S*)-**2** with (*S*)-**4** in the presence of K_2CO_3. Cyclization of *meso*-**5** with iminodiacetic acid affords (3*R*,5*S*)-3,5-dimethyl-1,4,7,10-tetraazacyclododecane-2,6-dione (*meso*-**6**). When reductive amination of *meso*-**6** was carried out using benzaldehyde and 3,5-difluorobenzaldehyde in the presence of $NaBH(OAc)_3$, 10-substituted derivatives (*meso*-**7a** and *meso*-**7b**) were obtained.

The X-ray structure of *meso*-**6** (Fig. 2) indicates that the N atom (at the 4-position in the cyclen) between the two methyl-substituted carbons does not react owing to the steric hindrance of the two neighboring methyl groups. A disubstituted compound, therefore, would not be obtained. After *meso*-**8a** and **8b** were obtained by the reduction of *meso*-**7a** and **7b**, the crude *meso*-**8a** and **8b** were used for reductive amination with benzaldehyde derivatives. Finally triple-armed cyclens (*meso*-**9a**–*meso*-**9d**) were obtained (Scheme 1).

The structure of an Ag^+ complex with *meso*-**9a** was examined from Ag^+-induced ^1H NMR chemical shift changes (Fig. 3). To assign the protons at the 2′- and 6′-positions in each aromatic ring, COSY, HMBC, and HMQC of a 1 : 1 (= *meso*-**9a**: Ag^+) mixture were measured (see Fig. S9–S12b in the ESI†). In addition, an analogue of *meso*-**9a** (*meso*-**9b**) bearing deuterated

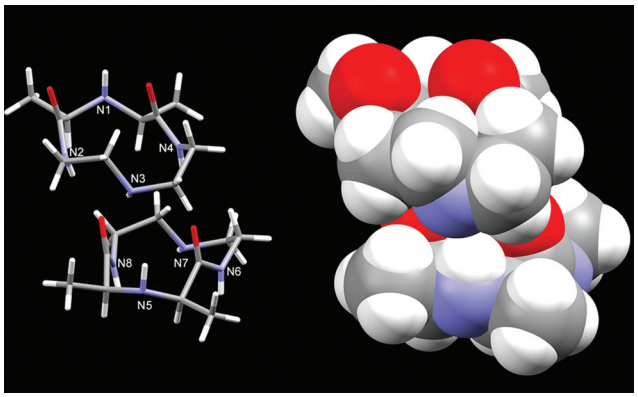

Fig. 2 X-ray structure of *meso*-**6**. Steric hindrance by the two methyl groups inhibits the reductive amination at the 10-position nitrogen (N1 and N5).

benzenes at the 1- and 7-positions was also prepared to clarify the chemical shift of the phenyl protons at the 10-position. As shown in Fig. 3, the aromatic H_a protons at the 10-position in the cyclen ring shifted to a higher field *ca.* by 0.74 ppm while the aromatic H_b protons at the 1- and 7-positions shifted to a higher field *ca.* by 0.13 ppm.

On the other hand, the H_a protons in *meso*-**9c** and *meso*-**9d** which have 3,5-difluorobenzenes at the 1- and 7-positions in the cyclen shifted to a higher field *ca.* by 0.36 ppm (Fig. 4). The H_b protons in *meso*-**9c** shifted to a higher field *ca.* by 0.13 ppm. The value is similar to that of H_b protons in *meso*-**9a**.

Fig. 5 shows electrostatic potential maps, calculated using the B3LYP/6-31G(*) method,[8] of toluene and 1,3-difluoro-4-methylbenzene. The electrostatic potential maps show that the electron densities in toluene are higher than those in 1,3-difluoro-4-methylbenzene. These chemical shift changes strongly support the fact that the chemical shift changes in the H_a and H_b protons are affected by the electron density on the aromatic rings next to them. These chemical shift changes are summarized in Table 1.

As we previously reported,[2c,d] the aromatic protons at the 2′- and 6′-positions of aromatic side-arms (the H_a protons in Fig. 1) in the tetra-armed cyclen bearing four phenyl groups shifted to a higher field *ca.* by 0.96 ppm. The higher field shift changes in the triple-armed cyclens indicate that the aromatic side-arms of *meso*-**9a–9d** cover the Ag^+ incorporated into the cyclen cavities. Small chemical shift changes of H_b protons at the 1- and 7-positions would be due to the absence of an aromatic side-arm at the 4-position nitrogen and rapid inversion between Δ and Λ enantiomers (Fig. 6). It is important to note that symbols Δ and Λ refer to the helicity of the pendant arms.

To estimate the inversion barrier between Δ and Λ forms of *meso*-**9b**, VT ^1H NMR experiments on a 1 : 1 mixture of *meso*-**9b** and Ag^+ in CD_2Cl_2–CD_3OD were carried out in the range of 293 K–193 K (Fig. 7).

As shown in Fig. 7, the coalescence temperature was observed at 243 K for the H_b protons in the phenyl rings at the 1- and 7-positions and the methyl protons. The inversion

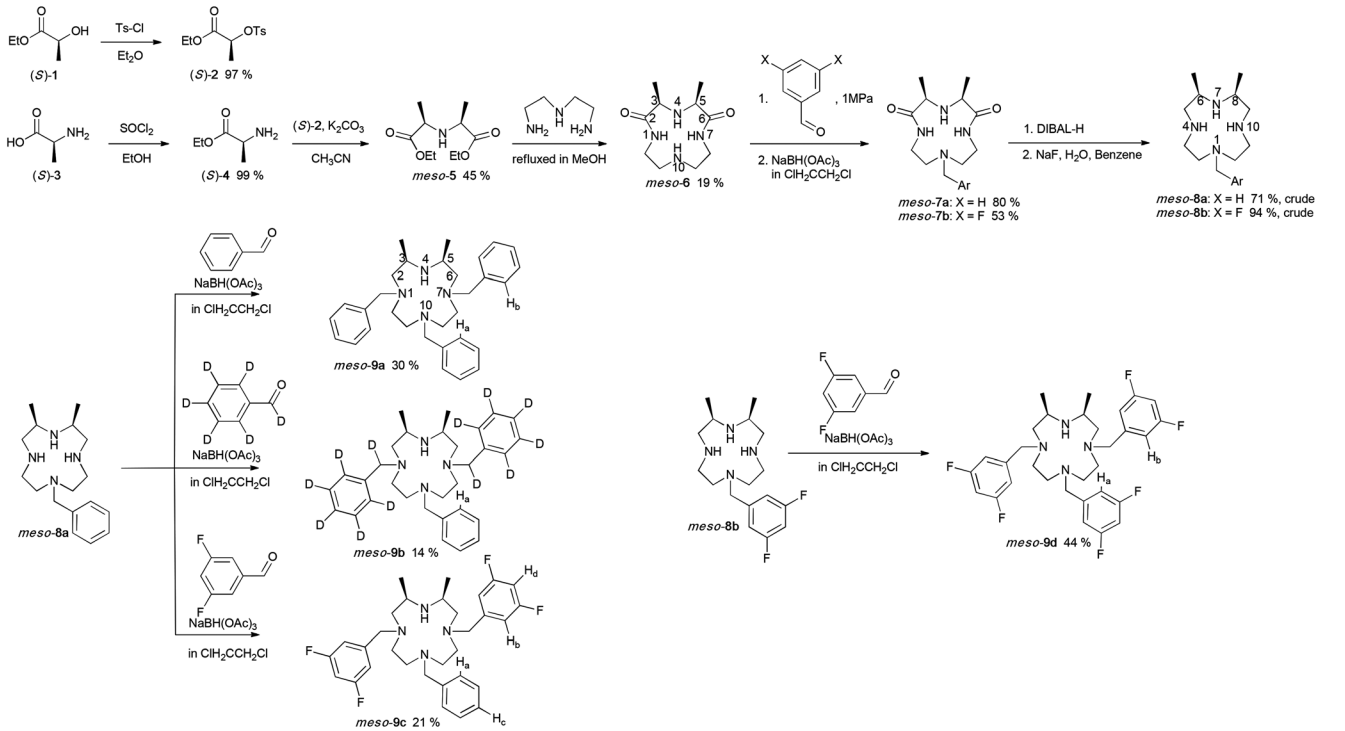

Scheme 1

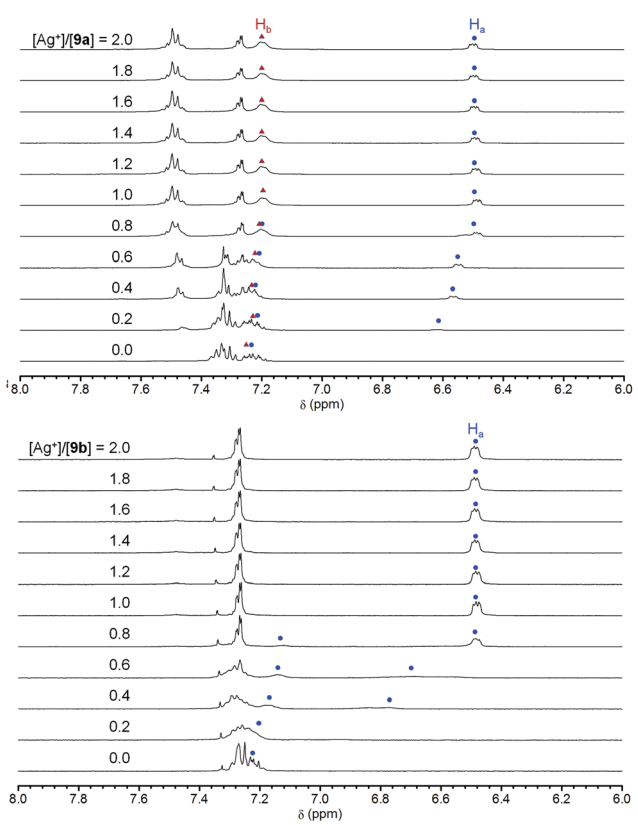

Fig. 3 Ag^+-induced ^1H NMR spectral changes of *meso*-**9c** (top) and *meso*-**9d** (bottom) in CD_2Cl_2–CD_3OD.

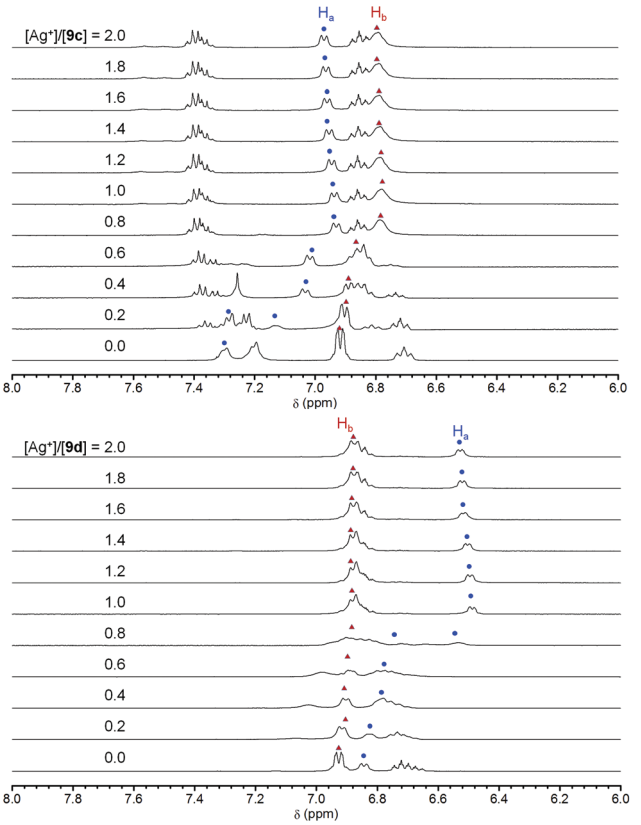

Fig. 4 Ag^+-induced ^1H NMR spectral changes of *meso*-**9c** (top) and *meso*-**9d** (bottom) in CD_2Cl_2–CD_3OD.

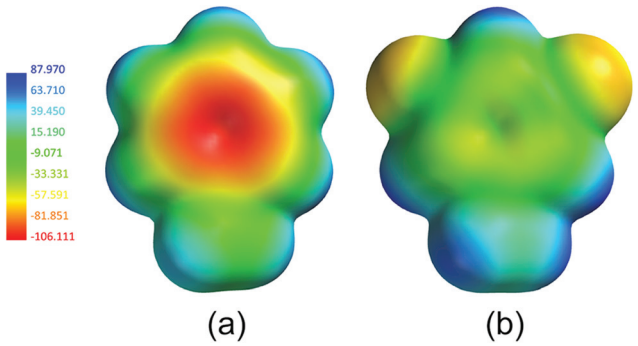

Fig. 5 Electrostatic potential maps of (a) toluene and (b) 1,3-difluoro-4-methylbenzene (property range: kJ mol^{-1}).

Table 1 Ag$^+$-induced-^{1}H NMR chemical shift changes (Δ ppm)[a]

Compd.	H_a (10-position)	H_b (1- and 7-positions)
meso-**9a**	−0.7	−0.13
meso-**9b**	−0.74	—
meso-**9c**	−0.36	−0.13
meso-**9d**	−0.36	−0.04

[a] Negative values mean higher field shift.

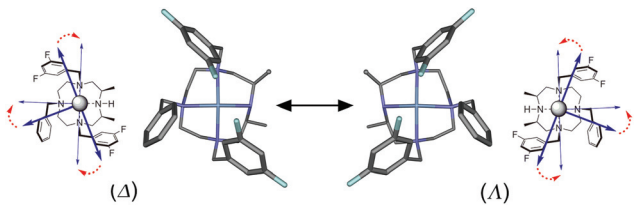

Fig. 6 Optimized structures of Δ and Λ enantiomers of the *meso*-**9b**/Ag$^+$ complex (B3LYP/6-31G*). Hydrogen atoms are omitted for clarity.

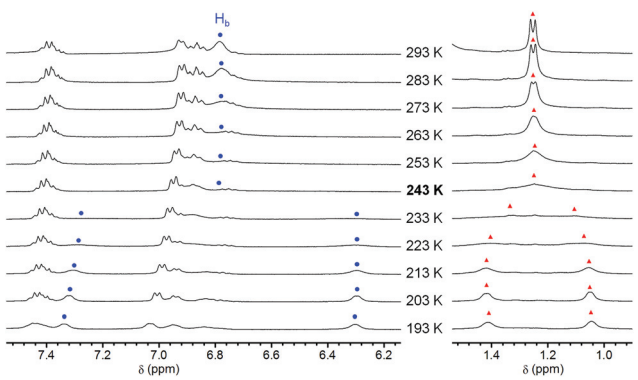

Fig. 7 VT ^{1}H NMR experiments of *meso*-**9b**/Ag$^+$ in CD_2Cl_2–CD_3OD.

barrier ($\Delta G^{\ddagger}$) was estimated to be 11 kcal mol^{-1} using the methodology previously described by Shanan-Atidi and Bar-Eli.[9] This is the first example of an inversion barrier in Ag$^+$ complexes with double-, triple-, and tetra-armed cyclens.

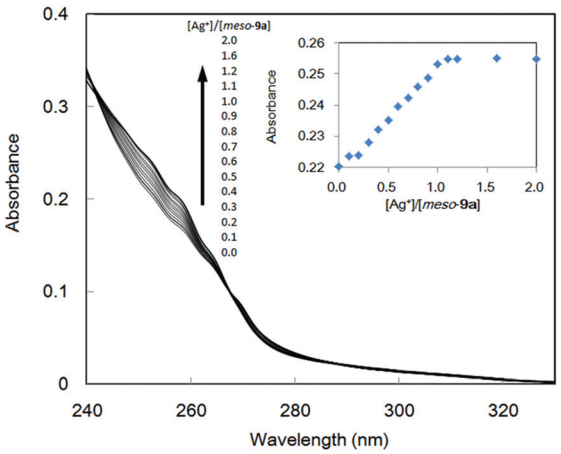

Fig. 8 Ag$^+$-induced-UV-vis spectral changes of *meso*-**9a**/Ag$^+$ in CH_3CN.

Titration experiments using UV spectra were carried out to confirm the Ag$^+$–π interactions in CH_3CN. Fig. 7 shows the Ag$^+$-ion-induced UV spectral changes in *meso*-**9a** (and Fig. S25 and S26 in the ESI† for *meso*-**9c** and *meso*-**9d**, respectively). An increase in the absorbance between 242 and 267 nm was observed with isosbestic points at 242 and 267 nm, upon the addition of Ag$^+$. An inflection point was observed at 1.0 (= [Ag$^+$]/[*meso*-**9a**]), showing a 1 : 1 complex (Fig. 8). Nonlinear least-squares analyses of the titration profiles clearly indicated the formation of a 1 : 1 complex, and allowed us to estimate the association constants defined as eqn (1). The log K values between the ligands (*meso*-**9a**, *meso*-**9c** and *meso*-**9d**) and Ag$^+$ in CH_3CN were estimated to be *ca.* 5.6, 6.5, and 6.5, respectively, using the HYPERSPC calculation program.[10]

$$\text{Ligand} + \text{Ag}^+ \rightleftharpoons [\text{Ligand} - \text{Ag}^+]$$
$$K = [\text{Ligand} - \text{Ag}^+]/[\text{Ligand}][\text{Ag}^+] \quad (1)$$

X-ray structures of Ag$^+$ complexes with the triple-armed cyclens were measured (Fig. 9). In *meso*-**9b**/$AgPF_6$, three side-arms cover the Ag$^+$ and the C13–Ag1, C20–Ag1, and C27–Ag1 distances are 3.709, 3.179, and 3.613 Å, respectively. We

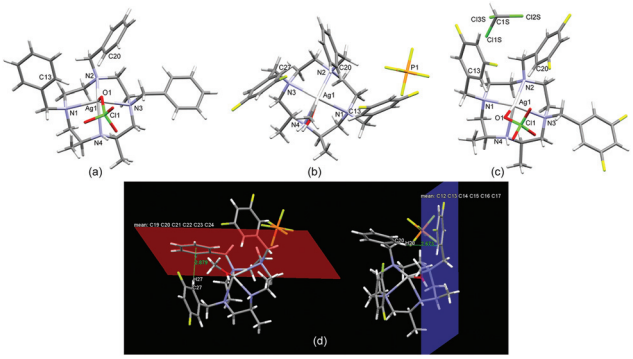

Fig. 9 X-ray structures of (a) *meso*-**9a**/$AgClO_4$, (b) *meso*-**9c**/$AgPF_6$, (c) *meso*-**9d**/$AgClO_4$, and (d) C–H–plane distances of *meso*-**9c**/$AgPF_6$.

reported that the typical C–Ag distance range in tetra-armed cyclens is 3.272–3.344 Å,[2b,d] and the 3.6–3.7 Å is a relatively long distance range. These longer distances would be due to the absence of an aromatic side-arm at the 4-position nitrogen. In addition, intramolecular CH–π interactions between the aromatic rings are also observed in the *meso*-**9b**/$AgPF_6$ complex (Fig. 9d). The H20–benzene plane (C12 to C17) and the H27–benzene plane (C19 to C24) distances are 2.673 and 2.879 Å, respectively. These distances are comparable to typical CH–π distances in aromatic rings.[11] On the other hand, in the *meso*-**9a**/$AgClO_4$ (Fig. 9a) and *meso*-**9c**/$AgClO_4$ (Fig. 9c) complexes, two aromatic side-arms at the 1- and 10-positions cover the Ag^+, while the third side-arm at the 7-position does not. The Ag–ClO_4 bond lengths of the *meso*-**9a**/$AgClO_4$ (Fig. 9a) and *meso*-**9c**/$AgClO_4$ are in the range 2.344–2.600 Å. These distances are typical Ag–ClO_4 bond distances.[3a,12] The coordination of ClO_4^- to the Ag^+ bond prevents the Ag^+–π interaction in the solid state. Interestingly, the mean average derivations of Ag^+–N distances in the Ag^+ complexes with **9a**, **9b**, and **9c** are greater than those of tetra-armed cyclens previously reported (Table 1S in the ESI†). These deviations mean that the cyclen rings are distorted in the Ag^+ complexes with triple-armed cyclens. The smaller $\log K$ values of the triple-armed cyclens ($\log K$ = 5.6–6.5) than those of tetra-armed cyclens ($\log K$ = 6.8)[2c,e] would be due to the ring distortion.

To visualize the Ag^+–π interactions, the LUMOs and HOMOs were calculated by the DFT method [B3LYP/3-21G(*)] using the X-ray structures of the *meso*-**9c**/$AgPF_6$ complex. As shown in Fig. 10, the LUMO of Ag^+ is in contact with the HOMOs of the aromatic side-arms. However, in this case, significant distortion of the LUMO like tetra-armed cyclen/Ag^+ complexes was not observed. This result indicates that the Ag^+–π interactions in the triple-armed cyclen/Ag^+ complex would not be very strong.

Conclusions

In the introduction part, we raised three questions about triple-armed cyclens. Now we can answer the questions as follows: (i) the ^{1}H NMR and UV-vis titration experiments showed that the triple-armed cyclens behave like an insectivorous plant (Venus flytrap), thus the three aromatic side-arms cover the Ag+ incorporated into the cyclen cavities. X-ray structures exhibited that Ag^+–π interactions as well as C–H–π interactions are crucial for triple-armed cyclens to work as argentivorous molecules. (ii) When two kinds of aromatic rings are introduced as side-arms, the chemical shift of the protons at the 2′- and 6′-positions in the side-arms changed systematically depending on the next neighboring benzene. (iii) The inversion barrier between *Δ* and *Λ* forms of *meso*-**9b** was estimated to be 11 kcal mol^{-1} by VT ^{1}H NMR studies. Synthesis, the complexing property towards Ag^+, and chiral enhancement by chiral argentivorous molecules are now in progress in our laboratory.

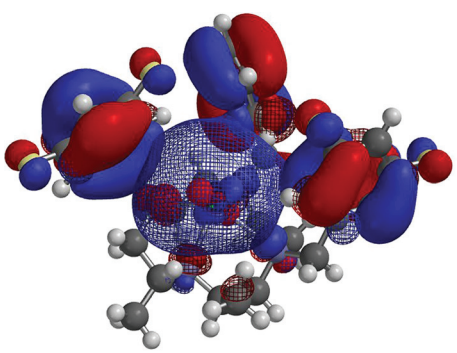

Fig. 10 The LUMO and HOMOs calculated by the DFT method [B3LYP/3-21G(*)] using the X-ray structures of the *meso*-**9c**/Ag^+ complex (isosurface value is 0.02 au). LUMO (mesh) and HOMO[−4], HOMO[−5], and HOMO[−7] (solid).

Experimental section

General information

Melting points were obtained with Mel-Temp capillary apparatus and were not corrected. FAB mass spectra were obtained using a JEOL 600 H mass spectrometer. ^{1}H NMR spectra were measured in $CDCl_3$, CD_2Cl_2, or a mixture of CD_2Cl_2 and CD_3OD on a JEOL ECP400 (400 MHz) spectrometer. UV-vis spectra were recorded on a JASCO V-550 spectrometer. The elemental analysis was carried out on a Yanako MT-6 CHN Micro Corder. All reagents were of standard analytical grade and were used without further purification. Optical rotations were measured on a digital polarimeter JASCO DIP-360.

Ethyl(*S*)-2-[[(4-methylphenyl)sulfonyl]oxy]propionate (*S*)-2. (*S*)-**2** was prepared according to the literature.[5] Yield 97%. Pale yellow oil. $[\alpha]_D$ = −30.5 (c = 2.69, $CHCl_3$). ^{1}H NMR ($CDCl_3$): δ 7.82 (d, J = 8.2 Hz, 2H), 7.35 (d, J = 8.2 Hz, 2H), 4.93 (q, J = 7.1 Hz, 1H), 4.12 (dq, J_1 = 7.1 Hz, J_2 = 1.1 Hz, 2H), 2.45 (s, 3H), 1.51 (d, J = 7.1 Hz, 3H), 1.21 (t, J = 7.1 Hz, 3H). FAB-MS (m/z) (matrix: dithiothreitol (DTT)–α-thioglycerol (TG) = 1 : 1): 273 ($[M + 1]^+$, 100%).

Ethyl L-alaninate hydrochloride (*S*)-4. (*S*)-**4** was prepared according to the literature.[6] Yield 99%. Mp: 77.0–79.0 °C. $[\alpha]_D$ = +3.2 (c = 2.41, CH_3OH). ^{1}H NMR($CDCl_3$): δ 8.75 (s, 3H), 4.30–4.20 (m, 3H), 1.73 (d, J = 7.1 Hz, 3H), 1.30 (t, J = 7.1 Hz, 3H). FAB-MS (m/z) (matrix: DTT–TG = 1 : 2): 154 ($[M + 1 - HCl]^+$, 100%).

Diethyl (2*R*,2′*S*)-2,2′-iminodipropanoate *meso*-5. *meso*-**5** was prepared according to the literature.[7] Yield 45%. Colorless oil. ^{1}H NMR ($CDCl_3$): δ 4.22–4.11 (m, 4H), 3.38 (q, J = 7.0 Hz, 2H), 1.31 (d, J = 7.1 Hz, 6H), 1.28 (t, J = 7.1 Hz, 6H). FAB-MS (m/z) (matrix: DTT–TG = 1 : 1): 218 ($[M + 1]^+$, 100%).

(3*R*,5*S*)-3,5-Dimethyl-1,4,7,10-tetraazacyclododecane-2,6-dione *meso*-6. *meso*-**5** (2.19 g, 10.1 mmol) was dissolved in absolute CH_3OH (250 mL) and then added to a solution of diethylenetriamine (1.05 g, 10.2 mmol) in 250 mL absolute MeOH. The reaction mixture was stirred at 70 °C under an argon atmosphere for 7 days, and then the solvent was removed under reduced pressure. *meso*-**6** was obtained as white powder by

recrystallization from a mixture of acetonitrile and methanol. Yield 19%. White solid. Mp: 191–194 °C. ^{1}H NMR ($CDCl_3$): δ 3.55–3.47 (m, 2H), 3.20 (q, J = 7.0 Hz, 2H), 3.07–3.00 (m, 2H), 2.95–2.89 (m, 2H), 2.67–2.61 (m, 2H), 1.37 (d, J = 7.0 Hz, 6H). FAB-MS (m/z) (matrix: DTT–TG = 1 : 2): 229 ($[M + 1]^+$, 100%). Anal. calcd for $C_{10}H_{20}N_4O_2$ + 1/10H_2O: C, 52.20; H, 8.85; N, 24.35. Found: C, 52.20; H, 8.85; N, 24.35.

(3*R*,5*S*)-10-Benzyl-3,5-dimethyl-1,4,7,10-tetraazacyclododecane-2,6-dione *meso*-7a. After a mixture of *meso*-**6** (684 mg, 3.00 mmol) and benzaldehydes (1.13 g, 10.6 mmol) in 1,2-dichloroethane was stirred for 24 h at 1 MPa (argon atmosphere), $NaBH(OAc)_3$ (1.91 g, 9.00 mmol) was added and stirred for 24 h at atmospheric pressure (argon atmosphere). To the reaction mixture, saturated aqueous $NaHCO_3$ was added, and the organic layer was separated. The aqueous layer was extracted with $CHCl_3$ (50 mL × 3). The combined organic layer was washed with water, dried over Na_2SO_4, and concentrated. The residual solid was recrystallized from acetonitrile to give *meso*-**7a** as a white solid. Yield 0.763 g (80%). Mp: 174–177 °C. ^{1}H NMR ($CDCl_3$): δ 7.39–7.23 (m, 5H), 3.70 (s, 2H), 3.50–3.45 (m, 2H), 3.22 (q, J = 7.0 Hz, 2H), 3.04–3.97 (m, 2H), 2.62 (t, J = 5.7 Hz, 4H), 1.37 (d, J = 7.0 Hz, 6H). FAB-MS (m/z) (matrix: DTT–TG = 1 : 2): 319 ($[M + 1]^+$, 100%). Anal. Calcd for $C_{17}H_{26}N_4O_2$: C, 64.12; H, 8.23; N, 17.60. Found: C, 64.36; H, 8.27; N, 17.84.

(3*R*,5*S*)-10-(3,5-Difluorobenzyl)-3,5-dimethyl-1,4,7,10-tetraazacyclododecane-2,6-dione *meso*-7b. *meso*-**7b** was prepared in a similar manner with the synthetic procedure of *meso*-**7a**. Yield 53%. White solid. Mp: 198–201 °C. ^{1}H NMR ($CDCl_3$): δ 6.98–6.88 (dd, J = 8.3 Hz, 2H), 6.77–6.73 (m, 1H), 3.68 (s, 1H), 3.53–3.45 (m, 2H), 3.25–3.20 (q, J = 7.1 Hz 2H), 3.13–3.06 (m, 2H), 2.67–2.55 (m, 4H), 1.38 (d, J = 7.1 Hz, 6H). FAB-MS (m/z) (matrix: DTT–TG = 1 : 2): 355 ($[M + 1]^+$, 100%). Anal. Calcd for $C_{17}H_{24}N_4F_2O_2$: C, 57.61; H, 6.83; N, 15.81. Found: C, 57.70; H, 6.71; N, 15.49.

(6*R*,8*S*)-1-Benzyl-6,8-dimethyl-1,4,7,10-tetraazacyclododecane *meso*-8a. A mixture of *meso*-**7a** (0.637 g, 2.00 mmol) and DIBAL-H (10 mL, 1 M solution in THF) was stirred at 0 °C under an argon atmosphere for 1 day. After NaF (3.35 g, 80.0 mmol) in water (1 mL) and benzene (60 mL) was added at 0 °C, the mixture was stirred for 5 h. The reaction mixture was filtered, and the filtrate was concentrated under reduced pressure. Crude *meso*-**8a** was used without further purification. Yield 0.413 g (71%). Mp: 89–93 °C. ^{1}H NMR ($CDCl_3$): δ 7.35–7.20 (m, 5H), 3.62 (s, 2H), 2.94 (br-s, 2H), 2.70–2.47 (m, 10H), 2.38–2.27 (m, 2H), 1.11 (d, J = 7.0 Hz, 6H). FAB-MS (m/z) (matrix: DTT–TG = 1 : 2): 291 ($[M + 1]^+$, 100%).

(6*R*,8*S*)-1-(3,5-Difluorobenzyl)-6,8-dimethyl-1,4,7,10-tetraazacyclododecane *meso*-8b. *meso*-**8b** was prepared in a similar manner with the synthetic procedure of *meso*-**8a** using *meso*-**7b**. Yield 0.306 g (94%). Mp: 83–86 °C. ^{1}H NMR ($CDCl_3$) δ 6.88 (d, J = 8.6 Hz, 2H), 6.67 (t, J = 8.6 Hz, 1H), 3.60 (s, 2H), 2.98–2.90 (m, 2H), 2.71–2.56 (m, 8H), 2.55–2.47 (m, 2H), 2.40–2.33 (dd, J_1 = 5.6 Hz, J_2 = 6.5, 2H), 1.12 (d, J = 6.5 Hz, 6H). FAB-MS (m/z) (matrix: DTT–TG = 1 : 1): 327 ($[M + 1]^+$, 100%).

(3*R*,5*S*)-1,7,10-Tribenzyl-3,5-dimethyl-1,4,7,10-tetraazacyclododecane *meso*-9a. After a mixture of *meso*-**8a** (294 mg, 1.01 mmol), benzaldehydes (633 mg, 5.96 mmol), and $NaBH(OAc)_3$ (1.27 g, 5.99 mmol) in 1,2-dichloroethane (10 mL) was stirred for 5 days at rt under an argon atmosphere (atmospheric pressure), saturated aqueous $NaHCO_3$ was added. The organic layer was separated, and the aqueous layer was extracted with $CHCl_3$ (50 mL × 3). The combined organic layer was washed with water, dried over Na_2SO_4, and concentrated. The residual oil was separated and purified by column chromatography on silica-gel ($CHCl_3$–MeOH–NH_3 aq = 5/1/0.06) to give *meso*-**9a** as a pale-yellow oil. Yield 0.142 g (30%). Pale-yellow oil. ^{1}H NMR (CD_2Cl_2): δ 7.37–7.29 (m, 10H), 7.26–7.19 (m, 5H), 3.82 (d, J = 14.0 Hz, 2H), 3.50 (s, 2H), 3.41 (d, J = 14.0 Hz, 2H), 2.93–2.88 (br, 2H), 2.74–2.60 (m, 4H), 2.49–2.39 (m, 6H), 2.28 (d, J = 14.0 Hz, 2H), 0.95 (d, J = 6.5 Hz, 6H). Anal. Calcd for $C_{31}H_{42}N_4$ + 0.25CH_3OH: C, 78.41; H, 9.05; N, 11.70. Found: C, 78.71; H, 8.86; N, 11.33. FAB-MS (m/z) (matrix: DTT–TG = 1 : 1): 471 ($[M + 1]^+$, 100%).

(3*R*,5*S*)-10-Benzyl-3,5-dimethyl-1,7-bis[($^2H_5$)phenyl($^2H_1$)methyl]-1,4,7,10-tetraazacyclododecane *meso*-9b. *meso*-**9b** was prepared in a similar manner with the synthetic procedure of *meso*-**9a** using *meso*-**8a** and benzaldehyde-d_6. Yield 14%. Brown oil. ^{1}H NMR (CD_2Cl_2): δ 7.34–7.18 (m. 5H), 3.82 (s, 0.7H), 3.54 (s, 3.3H), 2.98–2.85 (m, 2H), 2.81–2.47 (m, 8H), 2.46–2.31 (m, 4H), 1.11 (d, J = 6.2 Hz, 6H). MS (m/z) (matrix: DTT–TG = 1 : 1): 483 ($[M + 1]^+$, 100%). Anal. Calcd for $C_{31}H_{29}D_{12}N_4$ + H_2O: C, 74.50; H, 6.25; D, 4.84; N, 11.21. The thermal conductivity of hydrogen is almost the same as that of deuterium. Apparent H% is calculated using the following equation: $H_{apparent}\% = H_{calcd}\% + D_{calcd}\%/2 = 6.25\% + (4.84/2)\% = 8.67\%$, where H_{calcd}% and D_{calcd}% are calculated H%, and calculated D%, respectively. Therefore, C, 74.50; H, 8.67; N, 11.21. Found: C, 74.49; H, 8.64; N, 10.88.

(3*R*,5*S*)-10-Benzyl-1,7-bis(3,5-difluorobenzyl)-3,5-dimethyl-1,4,7,10-tetraazacyclododecane *meso*-9c. *meso*-**9c** was prepared in a similar manner with the synthetic procedure of *meso*-**9a** using *meso*-**8a** and 3,5-difluorobenzaldehyde. Yield 21%. Pale yellow solid. Mp: 90.0–91.5 °C. ^{1}H NMR (CD_2Cl_2): δ 7.35–7.26 (m, 2H), 7.24–7.14 (m, 3H), 6.92 (d, J = 8.7 Hz, 5H), 6.71 (t, J = 8.7 Hz, 2H), 3.80 (d, J = 15.0 Hz, 2H), 3.54 (d, J = 15.0 Hz, 2H), 3.48 (s, 2H), 2.86 (br-s, 2H), 2.77–2.67 (m, 2H), 2.61–2.47 (m, 6H), 2.47–2.33 (m, 4H), 0.96 (br-s, 6H). MS (m/z) (matrix: DTT–TG = 1 : 1): 543 ($[M + 1]^+$, 100%). Anal. Calcd for $C_{31}H_{38}F_4N_4$ + H_2O: C, 68.61; H, 7.06; N, 10.32. Found: C, 68.70; H, 7.07; N, 10.22.

(3*R*,5*S*)-1,7,10-Tris(3,5-difluorobenzyl)-3,5-dimethyl-1,4,7,10-tetraazacyclododecane *meso*-9d. *meso*-**9d** was prepared in a similar manner with the synthetic procedure of *meso*-**9a** using *meso*-**8b** and 3,5-difluorobenzaldehyde. Yield 44%. Pale yellow solid. Mp: 83.0–86.0 °C. ^{1}H NMR (CD_2Cl_2): δ 6.93 (d, J = 9.1 Hz, 4H), 6.84 (d, J = 9.1 Hz, 2H), 6.72 (t, J = 9.1 Hz, 2H), 6.67 (t, J = 9.1 Hz, 1H), 3.85 (J = 15.3 Hz, 2H), 3.62 (J = 15.3 Hz, 2H), 3.48 (s, 2H), 3.66 (s, 1H), 2.95–2.83 (m, 2H), 2.82–2.69 (m, 4H), 2.68–2.56 (m, 4H), 2.56–2.38 (m, 4H), 1.18–0.99 (br-s, 6H). MS (m/z) (matrix: DTT–TG = 1 : 1): 579 ($[M + 1]^+$, 100%). Anal.

Table 2 Crystal data of *meso*-**6**, *meso*-**9a**/$AgClO_4$, *meso*-**9b**/$AgPF_6$, and *meso*-**9c**/$AgClO_4$

Compound	*meso*-**6**	*meso*-**9a**/$AgClO_4$	*meso*-**9b**/$AgPF_6$	*meso*-**9c**/$AgClO_4$
Formula	$C_{10}H_{20}N_4O_2$	$C_{31}H_{44}AgClN_4O_5$	$C_{32}H_{42}AgF_{10}N_4OP$	$C_{32}H_{37}AgCl_4N_4O_4$
M	228.30	696.02	827.54	905.33
T/K	273	173	90	120
Crystal system	Monoclinic	Monoclinic	Monoclinic	Monoclinic
Space group	$P2(1)/c$	$P2(1)$	$P2(1)/c$	$P2(1)/c$
a/Å	9.6821(6)	8.8291(4)	10.6718(6)	19.0094(10)
b/Å	16.7879(10)	20.5803(10)	15.1390(9)	9.2229(5)
c/Å	14.9185(9)	17.8396(8)	23.2571(11)	22.7450(12)
β/°	102.0980(10)	94.1870(10)	116.497(2)	113.5130(10)
U/Å^3	2371.0(2)	3232.9(3)	3362.7(3)	3656.6(3)
Z	8	4	4	4
D_c/g cm^{-3}	1.279	1.430	1.635	1.645
μ/mm^{-1}	0.091	0.750	0.736	0.917
Data/restraints/parameters	6611/0/325	12 943/107/769	7688/0/453	9097/0/466
No. reflns used [$>2\sigma(I)$]	6611 [R(int) = 0.0354]	12 943 [R(int) = 0.0168]	7688 [R(int) = 0.0234]	9097 [R(int) = 0.0268]
R_1, wR_2 [$I > 2\sigma(I)$]	0.0499, 0.1162	0.0322, 0.0874	0.0314, 0.0822	0.0329, 0.0857
R_1, wR_2 [all data]	0.0754, 0.1282	0.0347, 0.0941	0.0341, 0.0857	0.0403, 0.0965
Absolute structure parameter		−0.033(16)		
GOF	1.030	1.076	1.051	1.130

Calcd for $C_{31}H_{36}F_6N_4$ + 1/2H_2O: C, 63.36; H, 6.35; N, 9.53. Found: C, 63.13; H, 6.15; N, 9.16.

Preparation of silver ion complexes. The ligand (0.0151 mmol) in chloroform or dichloromethane (1 mL) was added to the corresponding metal salt ($AgPF_6$ or $AgClO_4$) (0.0153 mmol) in methanol (1 mL). Crystals were obtained quantitatively on evaporation of the solvent.

meso-**9a**/$AgClO_4$. Mp: 112–115 °C (Dec.). Anal. Calcd for $C_{31}H_{42}AgClN_4O_4$ + 0.25H_2O: C, 54.55; H, 6.28; N, 8.21. Found: C, 54.50; H, 6.25; N, 8.20.

meso-**9b**/$AgPF_6$. Mp: 130–133 °C (Dec.). Anal. Calcd for $C_{31}H_{38}F_{10}N_4AgP$ + CH_3OH: C, 46.45; H, 5.12; N, 6.77. Found: C, 46.79; H, 5.06; N, 6.42.

meso-**9c**/$AgClO_4$. Mp: 143–145 °C (Dec.). Anal. Calcd for $C_{31}H_{36}AgClF_6N_4O_4$ + 0.1$CHCl_3$: C, 46.82; H, 4.56; N, 7.02. Found: C, 46.97; H, 4.88; N, 6.85.

^{1}H NMR titration experiments. ^{1}H NMR titration experiments were carried out at 298 K by the addition of 0.2–2.0 equivalents of $AgPF_6$ (1 mmol μL^{-1}) in CD_3OD to ligands (5×10^{-3} mmol/0.65 mL) in CD_2Cl_2.

UV-vis titration experiments. UV-vis titration experiments were carried out by addition of 0.1–2.0 equivalents of $AgPF_6$ in CH_3CN (3.0×10^{-2} M) to ligands in CH_3CN (1.0×10^{-4} M, 3 mL) at 298 K.

X-ray crystallography. Crystals of *meso*-**6**, *meso*-**9a**/$AgClO_4$, *meso*-**9b**/$AgPF_6$, and *meso*-**9c**/$AgClO_4$ were mounted on top of a glass fiber, and data collection was performed using a Bruker SMART CCD area diffractometer at 90–273 K. Data were corrected for Lorentz and polarization effects, and absorption corrections were applied using the SADABS[13] program. Structures were solved by direct methods and subsequent difference-Fourier syntheses using the program SHELEX.[14] All non-hydrogen atoms were refined anisotropically and hydrogen atoms were placed at the calculated positions and then refined using U_{iso}(H) = 1.2U_{eq}(C). The crystallographic refinement parameters of the complexes are summarized in Table 2.

Acknowledgements

The authors thank Professor Masatoshi Hasegawa for the TG DTA measurements. This research was supported by Grants-in-Aid 08026969, 11011761 and 26410100, a High-Tech Research Center project (2005–2009), and the Supported Program for Strategic Research Foundation at Private Universities (2012–2016) from the Ministry of Education, Culture, Sports, Science and Technology of Japan for Y.H.

Notes and references

1 (*a*) S. Shinoda, *Chem. Soc. Rev.*, 2013, **42**, 1825–1835; (*b*) C. Platas-Iglesias, *Eur. J. Inorg. Chem.*, 2012, **2012**, 2023–2033; (*c*) A. Rodríguez-Rodríguez, D. Esteban-Gómez, A. de Blas, T. Rodríguez-Blas, M. Fekete, M. Botta, R. Tripier and C. Platas-Iglesias, *Inorg. Chem.*, 2012, **51**, 2509–2521; (*d*) B. P. Burke, G. S. Clemente and S. J. Archibald, *J. Labelled Compd. Radiopharm.*, 2014, **57**, 239–243; (*e*) T. Y. Lee and J. Suh, *Pure Appl. Chem.*, 2009, **81**, 255–262.

2 (*a*) Y. Habata, M. Ikeda, A. K. Sah, K. Noto and S. Kuwahara, *Inorg. Chem.*, 2013, **52**, 11697–11699; (*b*) Y. Habata, Y. Okeda, M. Ikeda and S. Kuwahara, *Org. Biomol. Chem.*, 2013, **11**, 4265–4270; (*c*) Y. Habata, Y. Oyama, M. Ikeda and S. Kuwahara, *Dalton Trans.*, 2013, **42**, 8212–8217; (*d*) Y. Habata, A. Taniguchi, M. Ikeda, T. Hiraoka, N. Matsuyama, S. Otsuka and S. Kuwahara, *Inorg. Chem.*, 2013, **52**, 2542–2549; (*e*) Y. Habata, M. Ikeda, S. Yamada, H. Takahashi, S. Ueno, T. Suzuki and S. Kuwahara, *Org. Lett.*, 2012, **14**, 4576–4579.

3 (*a*) G. A. Bowmaker, Effendy, M. Nitiatmodjo, B. W. Skelton and A. H. White, *Inorg. Chim. Acta*, 2005, **358**, 4327–4341; (*b*) M. Wen, M. Munakata, Y. Suenaga, T. Kuroda-Sowa, M. Maekawa and I. Kodai, *Polyhedron*, 2004, **23**, 2117–2123.

4 "Argentivorous" is different from "argentophilic". "Argentophilic" is used in the sense of Ag^{+}–Ag^{+} interactions. For example, (*a*) E. C. Constable, C. E. Housecroft, P. Kopecky, M. Neuburger and J. A. Zampese, *Inorg. Chem. Commun.*, 2013, **27**, 159–162; (*b*) G.-G. Luo, D.-L. Wu, L. Liu, S.-H. Wu, D.-X. Li, Z.-J. Xiao and J.-C. Dai, *J. Mol. Struct.*, 2012, **1014**, 92–96; (*c*) R. Santra, M. Garai, D. Mondal and K. Biradha, *Chemistry*, 2013, **19**, 489–493; (*d*) G. A. Senchyk, V. O. Bukhan'ko, A. B. Lysenko, H. Krautscheid, E. B. Rusanov, A. N. Chernega, M. Karbowiak and K. V. Domasevitch, *Inorg. Chem.*, 2012, **51**, 8025–8033; (*e*) A. Stephenson and M. D. Ward, *Chem. Commun.*, 2012, **48**, 3605–3607; (*f*) J. Xu, S. Gao, S. W. Ng and E. R. T. Tiekink, *Acta Crystallogr., Sect. E: Struct. Rep. Online*, 2012, **68**, m639–m640; (*g*) J. Xu, S. Gao, S. W. Ng and E. R. T. Tiekink, *Acta Crystallogr., Sect. E: Struct. Rep. Online*, 2012, **68**, m639–m640; (*h*) G. Yang, P. Baran, A. R. Martinez and R. G. Raptis, *Cryst. Growth Des.*, 2013, **13**, 264–269.

5 R. W. Brown, *J. Agric. Food Chem.*, 1990, **38**, 269–273.

6 T. Jakusch, A. Dornyei, I. Correia, L. M. Rodrigues, G. K. Toth, T. Kiss, J. C. Pessoa and S. Marcao, *Eur. J. Inorg. Chem.*, 2003, 2113–2122.

7 S. S. Insaf and D. T. Witiak, *Tetrahedron*, 2000, **56**, 2359–2367.

8 (*a*) *Spartan'10*, Wavefunction, Inc., Irvine, CA; (*b*) W. J. Hehre, J. Yu, P. E. Klunzinger and L. Lou, *A Brief Guide to Molecular Mechanics and Quantum Chemistry Calculations*, Wavefunction, Irvine, CA, 1998, p. 159.

9 H. Shanan-Atidi and K. H. Bar-Eli, *J. Phys. Chem.*, 1970, **74**, 961–963.

10 P. Gans, A. Sabatini and A. Vacca, *Talanta*, 1996, **43**, 1739–1753.

11 (*a*) M. Nishio, Y. Umezawa, M. Hirota and Y. Takeuchi, *Tetrahedron*, 1995, **51**, 8665–8701; (*b*) M. Abe, M. Eto, K. Yamaguchi, M. Yamasaki, J. Misaka, Y. Yoshitake, M. Otsuka and K. Harano, *Tetrahedron*, 2012, **68**, 3566–3576.

12 (*a*) D.-Z. Wang, *J. Mol. Struct.*, 2009, **929**, 128–133; (*b*) J. Y. Liu, Z. Y. Liu, J. J. Zhang, Y. Y. Wang, P. Yang, Y. Wang, B. Ding and B. X. J. Zhao, *CrystEngComm*, 2013, **15**, 6413–6423; (*c*) F. Jin, X.–F. Yang, S.-L. Li, Z. Zheng, Z.-P. Yu, L. Kong, F.-Y. Hao, J.-X. Yang, J.-Y. Wu, Y.-P. Tian and H.-P. Zhou, *CrystEngComm*, 2012, **14**, 8409–8417; (*d*) C. V. K. Sharma and R. D. Rogers, *Cryst. Eng.*, 1998, **1**, 19–38; (*e*) S.-M. Fang, S.-T. Ma, L.-Q. Guo, Q. Zhang, M. Hu, L.-M. Zhou, L.-J. Gao and C.-S. Liu, *Inorg. Chem. Commun.*, 2010, **13**, 139–144; (*f*) G.-l. Zheng, H.-J. Zhang, S.-Y. Song, Y.-Y. Li and H.-D. Guo, *Eur. J. Inorg. Chem.*, 2008, 1756–1759; (*g*) H. Wu, X.-W. Dong, H.-Y. Liu, J.-F. Ma, Y.-Y. Liu, Y.-Y. Liu and J. Yang, *Inorg. Chim. Acta*, 2011, **373**, 19–26; (*h*) R. H. Laye, *Inorg. Chim. Acta*, 2007, **360**, 439–447; (*i*) Z.-P. Deng, L.-N. Zhu, S. Gao, L.-H. Huo and S. W. Ng, *Cryst. Growth Des.*, 2008, **8**, 3277–3284; (*j*) B. N. Ahamed, M. Arunachalam and P. Ghosh, *Inorg. Chem.*, 2011, **50**, 4772–4780; (*k*) T. Mochida, K. Okazawa and R. Horikoshi, *Dalton Trans.*, 2006, 693–704; (*l*) Y.-B. Xie, C. Zhang, J.-R. Li and X.-H. Bu, *Dalton Trans.*, 2004, 562–569; (*m*) L. Wang, T. Tao, S.-J. Fu, C. Wang, W. Huang and X.-Z. You, *CrystEngComm*, 2011, **13**, 747–749; (*n*) Q. Sun, M. Wei, Y. Bai, C. He, Q. Meng and C. Duan, *Dalton Trans.*, 2007, 4089–4094; (*o*) G. Yang, S.-L. Zheng, X.-M. Chen, H. K. Lee, Z.-Y. Zhou and T. C. W. Mak, *Inorg. Chim. Acta*, 2000, **303**, 86–93; (*p*) N. J. Williams, W. Gan, J. H. Reibenspies and R. D. Hancock, *Inorg. Chem.*, 2009, **48**, 1407–1415.

13 SADABS, version 2.03; G. M. Sheldrick, *Program for adsorption correction of area detector frames*, Bruker AXS, Inc., Madison, WI, 1996.

14 SHELXTLTM, *version 5.1*, Bruker AXS, Inc., Madison, WI, 1997.

